Creating Discomfort Maps via Hand-held Human Feedback Interface for Robotic Shoulder Physiotherapy

Ravenberg, J.G.; Belli, I.; Prendergast, J.M.; Seth, A.; Peternel, L.

DOI
10.1109/IROS58592.2024.10801858

Publication date
2024

Document Version
Final published version

Published in
Proceedings of the IEEE/RSJ International Conference on Intelligent Robots and Systems (IROS 2024)

2024 IEEE/RSJ International Conference on Intelligent Robots and Systems (IROS)
October 14-18, 2024. Abu Dhabi, UAE

Creating Discomfort Maps via Hand-held Human Feedback Interface for Robotic Shoulder Physiotherapy

Jevon Ravenberg[1], Italo Belli[1,2], J. Micah Prendergast[1], Ajay Seth[2], and Luka Peternel[1]

***Abstract*— In this work, we propose a method of capturing the patient's discomfort during robotic shoulder physiotherapy, creating "discomfort maps". These maps depict the personalized distribution of discomfort that each patient perceived across their shoulder range of motion, facilitating both robotic devices and human therapists to account for patient-specific characteristics during the therapeutic process. Our system enables a patient to communicate and map discomfort in space and time during movement via a handheld push-button device, while interacting with a robotic physical therapy device capable of moving the patient and estimating their pose. We validated our method through human factors experiments simulating shoulder physiotherapy sessions with 10 healthy participants. To avoid the risk of injury to the participants and to allow for ground truth map information, we emulate perceived discomfort via an auditory signal. Our experimental apparatus enabled participants to reconstruct synthetic discomfort maps, demonstrating the feasibility of automatically capturing and storing patient discomfort during robotic physiotherapy.**

I. Introduction

Musculoskeletal injuries resulting from accidents, recreational activities, and aging are the primary contributors to disability and work impairment. Among these injuries, shoulder rotator-cuff (RC) tears stand out as one of the most prevalent, with an estimated prevalence rate of 22.1% in the general population and over 50% for individuals aged 60 and above [1]. Restoring shoulder mobility and functionality after RC injuries requires a patient to undergo a prolonged and costly physiotherapy process.

Due to the complexity of the shoulder mechanism and a lack of quantitative insights into the risks of re-injury, conventional practices in RC physiotherapy tend to be conservative, even when administered by expert physiotherapists [2]. This conservative approach limits the treatment range of motion (RoM), potentially prolonging the recovery process. Increasing RoM safely, however, can enhance recovery speed and completeness [3]. Additionally, administering physical therapy can be physically demanding for physiotherapists who typically treat many patients a day, one at a time. Demand on physiotherapists is exacerbated by the growing gap between the number of people with rehabilitative needs and the number of available physiotherapists, due in part to the aging population and decreasing availability of medical personnel [4].

Robotic-assisted rehabilitation can offer solutions to both the safety and delivery challenges of rotator-cuff-related physical therapy. Robotics assists in reducing the physical load on the physiotherapist by taking over the weight of the patient's limbs, and potentially enabling therapists to operate remotely or with multiple patients at once. Furthermore, robotic platforms can quantify the patient's condition as input into their control system, and communicate vital information to the therapist. For instance, the muscle effort of the patient can be estimated from electromyography (EMG) measurements [5], [6], while musculoskeletal models can give an accurate estimate of the actual internal properties of the human body, such as joint loading [7], muscle fatigue [8], muscle comfort [9], and muscle manipulability [10]. Previously, our group has used a musculoskeletal model of the human shoulder to estimate safe RoM for rehabilitation, identifying configurations where the strain in the RC tendons are indicative of increased re-injury risk [11], [12]. The

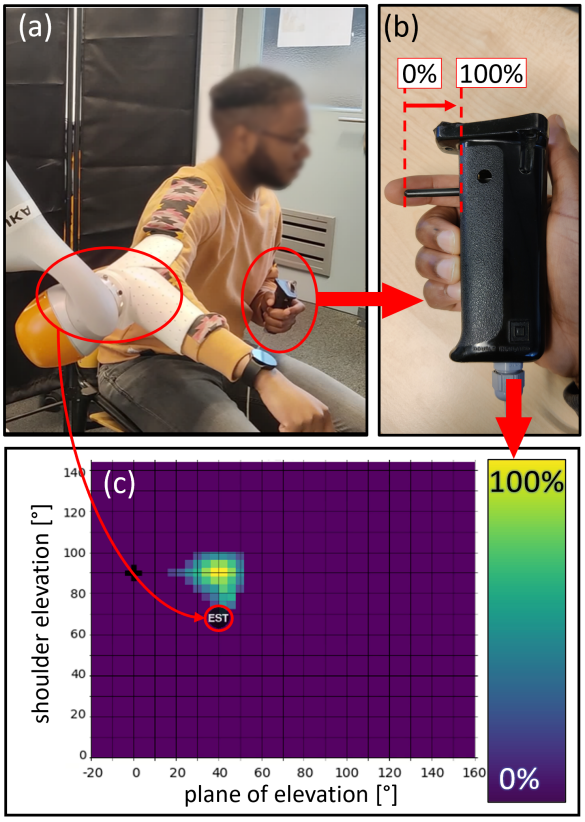

Fig. 1. Overview of the discomfort map creation system. (a) A KUKA LBR iiwa 7 R800 robotic manipulator acts as a physiotherapist and moves the participant's shoulder while simultaneously estimating their shoulder state. (b) A push-button interface (linear potentiometer), held by the free arm, is used to input discomfort intensity. (c) Example of a discomfort map created during the robotic shoulder physiotherapy.

Authors are with the Department of Cognitive Robotics[1] and the Department of BioMechanical Engineering[2], Delft University of Technology, Delft, The Netherlands (i.belli@tudelft.nl).

human RoM was abstracted into "strain maps", providing an intuitive representation of RC tendon strains and enabling more accurate monitoring of tendon strains by a physiotherapist and/or robotic system [11]–[13].

While model-based methods provide useful information about the patient's biomechanics, they do not quantify the patient's experience of discomfort or pain that might occur during a therapy session. Musculoskeletal models provide insights into mechanical variables like tendon strain, which are related to discomfort, but estimating discomfort itself remains challenging due to the wide variability among individuals, influenced by factors like inflammation and personal sensitivities. [14]. Despite being challenging, a patient's discomfort cannot be disregarded and methods to personalize therapy to the experience of discomfort are necessary for robot-mediated physiotherapy to be acceptable.

Perceived pain can be recorded based on physiological markers such as blood pressure, heart rate, and skin conductance [15], or behavioral responses such as facial expressions, which may be useful for informing machine learning algorithms [16]. Cheaper and more portable interfaces can allow the patient to log their perceived pain level directly, for example using a slider [17], [18], or single-handed grip devices as the input interfaces [19], [20], which could allow a therapist to compare the discomfort that the patient feels against subjective numerical ratings, e.g., the Numerical Rating Scale (NRS) [21]. In the rehabilitative robotics realm, limited work has addressed the problem of endowing robots with awareness about the pain/discomfort that their patients are experiencing. Perceived pain levels have been monitored after the therapy through the NRS [22], and online approaches have been designed with very precise hardware in mind [23] or proved to be challenging to generalize, requiring careful validation and training of the proposed pain-detecting algorithms [24].

Drawing inspiration from the interaction of physiotherapists and their patients, we propose a new method of integrating patient responses to perceived discomfort during robotic physiotherapy, to create "discomfort maps" that identify discomfort levels at different poses of the patient. Our main aim is to enable patients to autonomously provide their discomfort level in real-time during the robotic therapy session through a handheld push-button interface (see Fig. 1), and create discomfort maps that represent the discomfort distribution experienced over the RoM of the therapy. This information is inherently personalized to the patient and offers quantitative data, for informing both robot and human therapists about their patients' perceptions in real-time. By using a linear potentiometer as the push-button interface, our method combines the single-handed, intuitive nature of the grip interfaces with the more precise position-based and patient-agnostic continuous input of the slider.

The main contributions of this study are three-fold. 1) We present the concept of discomfort maps and introduce a novel combination of a handheld device with a collaborative robot to log patient discomfort during RC therapy as a function of their movements. 2) We validate our system through human factors experiments using auditory signals to emulate discomfort during movement, and measure user responses to test the accuracy of users to reconstruct a prescribed map. 3) Lastly, we propose that the subjective perception of discomfort could be used to enhance and further personalize other existing tools for robotic-assisted rehabilitation, such as the strain maps, and enable tracking of patient progress while unlocking new diagnostic opportunities.

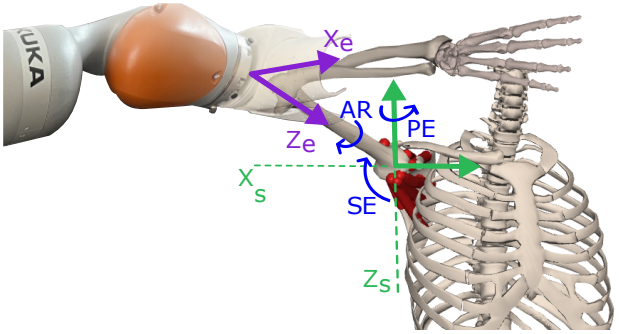

Fig. 2. Definitions of shoulder and end-effector coordinate reference frames. The shoulder frame (green), with the origin centered on the glenohumeral joint; DoF of the glenohumeral joint (blue); robot's end-effector frame (purple). When the patient is wearing the arm brace, the elbow frame coincides with the end-effector frame.

II. System Design

Our system is designed to allow the patient to input in real-time their level of perceived discomfort, as a continuous variable, using a push-button interface. Then, personalized discomfort maps are generated by relating the discomfort intensity to the current patient's shoulder state. To estimate the patient's shoulder state we employed a collaborative robot arm, which can also move the patient's shoulder through set trajectories (Fig. 1).

A. Shoulder State Definition

In the context of RC tendon rehabilitation, we define the shoulder state as the state of the glenohumeral joint [11], [12], i.e., the motion of the humerus (upper arm bone) relative to the scapula (shoulder blade), which has 3 degrees of freedom (DoF). As such, the shoulder state vector is defined as

$$\boldsymbol{\alpha} = [\text{AR PE SE}], \tag{1}$$

where AR $\in [-90°, 90°]$ is the axial rotation, PE $\in [-20°, 160°]$ is the shoulder plane of elevation, and SE $\in [0°, 144°]$ is the shoulder elevation. These coordinates are shown in Fig. 2. The state $[0°, 0°, 0°]$ coincides with the neutral pose where the arm rests at the side. The continuous shoulder range is discretized in 4° increments.

B. Discomfort Map

Similar to our previous efforts using strain maps [11], [12], we develop the idea of discomfort maps to indicate the intensity of a patient's discomfort over the RoM of interest. The idea behind the map creation is that the patient indicates shoulder configurations that cause discomfort, and the intensity of this discomfort. Our simultaneous logging of

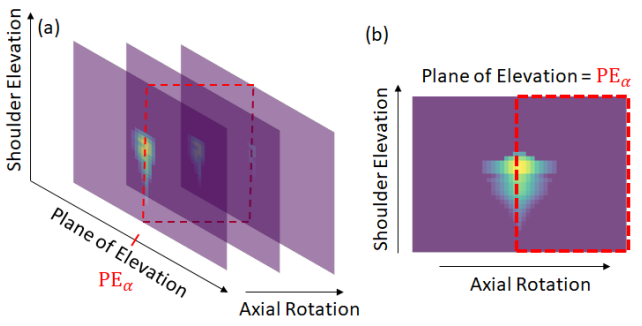

Fig. 3. Example of our discomfort maps: (a) maps for multiple values of AR layered on each other; (b) a cross-sectional view of the bounded area in (a), where the plane of elevation is at a fixed value of PE$_\alpha$. This demonstrates how the logged discomfort intensity dampens along the 3 DoF of the shoulder.

patient's discomfort and estimation of the patient's current shoulder state allows us to map the continuous, variable discomfort intensities directly onto the patient RoM, creating personalized discomfort maps. For visualization purposes, the 3D map of the patient's discomfort intensity level across AR, PE, and SE is represented as multiple layers of 2D maps, where AR is fixed. A single discomfort map shows the patient's discomfort intensity across PE and SE for a fixed AR, and by layering discomfort maps for all values of AR the entire shoulder RoM is spanned. An example of such maps is given in Fig. 3.

When creating a discomfort map, we assume that the perceived discomfort should not be specific to the current shoulder state, but also affect neighboring poses. Upon patient input, 3D ellipsoidal Gaussian clouds are logged in the discomfort maps, scaling them in amplitude and size with the intensity input, and centering them around the current shoulder state.

As such, the effect of the discomfort intensity $i(t)$ that the patient inputs on the information that the discomfort map carries at a generic shoulder state $\boldsymbol{\alpha}$ at time t is:

$$I(t,\boldsymbol{\alpha}) = \max\left(I(t-t_s,\boldsymbol{\alpha}),\ \ f(t,\boldsymbol{\alpha})\right), \tag{2}$$

$$f(t,\boldsymbol{\alpha}) = i(t)\prod_{j=1}^{3}\exp\left(-\frac{1}{2}\left(\frac{\alpha_j-\hat{\alpha}_j(t)}{\sigma_j(t)}\right)^2\right), \tag{3}$$

$$\boldsymbol{\sigma}(t) = i(t)\frac{1}{4}[w_{\text{AR}}\ w_{\text{PE}}\ w_{\text{SE}}] \tag{4}$$

where $I(t,\boldsymbol{\alpha})$ is the resulting discomfort level for shoulder state $\boldsymbol{\alpha}$ captured in the map at time t, t_s is the sampling time, $f(t,\boldsymbol{\alpha})$ describes the intensity distribution of the newest Gaussian cloud, $\hat{\boldsymbol{\alpha}}(t)$ is the estimated patient shoulder state, and $\boldsymbol{\sigma}(t)$ collects the standard deviations of such Gaussian cloud along the 3 DoF of the shoulder, proportional to input intensity through $[w_{\text{AR}}\ \ w_{\text{PE}}\ \ w_{\text{SE}}] = [60°\ \ 25°\ \ 25°]$. We selected a larger Gaussian cloud width in the AR direction since a rotation along AR corresponds to a relatively smaller movement of the arm, compared to equivalent rotations in PE and SE. This adjustment aims at augmenting the safety bounds along the DoF along which unnoticeable movement is more likely to happen. Equation (2) describes how the logged discomfort intensity for each shoulder state $\boldsymbol{\alpha}$ can only be overwritten by a Gaussian cloud with higher intensity. This stems from a conservative approach that regards the highest intensity input at the same shoulder state as the most representative.

C. Patient Input and Feedback Interfaces

The interface used for inputting discomfort intensity must enable the patient to instantly indicate not only whether and when they experience discomfort but also to quantify the level of such discomfort. Furthermore, the interface should be comfortable to hold for a long time and intuitive. To comply with these requirements, we use a handle with a spring-return linear potentiometer, already employed effectively in other human-robot interaction tasks [25] (Fig. 1.b). The discomfort intensity $i(t)$ input to the system scales linearly with the push-button position, ranging from 0% when fully extended to 100% when fully pushed in. The total allowable travel of the push-button is 2.5 cm, allowing for fine resolution in the discomfort logging. Further, participants held the handle in their free arm, to prevent the effects of involuntary muscle contractions due to the therapy on the button press.

D. Robot Control

A collaborative robot arm is used to estimate the shoulder state of the participant through the robot's built-in encoders, while also guiding the participant's shoulder through set trajectories. For estimating the human shoulder state, we follow the same approach as our previous work, as the shoulder angles are fully determined by the end-effector pose when the glenohumeral joint center does not move [11], [12]. During the experiments, we monitored our participants to satisfy this condition. To execute the experimental trajectories, an impedance controller is used, which takes the desired motion of the robot end-effector as an input and calculates the required robot joint torques based on mass-spring-damper equations [26]. Unlike fully stiff conventional position-controlled robots, the torque-controlled robot with an end-effector impedance controller can be compliant, which is crucial for safe human-robot interaction. The robot end-effector force and corresponding torques that generate that force are calculated with:

$$\boldsymbol{F} = \boldsymbol{K}(\boldsymbol{x}_r - \boldsymbol{x}) - \boldsymbol{D}(\dot{\boldsymbol{x}}_r - \dot{\boldsymbol{x}}) \tag{5}$$

$$\boldsymbol{\tau} = \boldsymbol{J}^T\boldsymbol{F} \tag{6}$$

where $\boldsymbol{F} \in \mathbb{R}^6$ is the output force, $\boldsymbol{K} \in \mathbb{R}^{6\times6}$ is the Cartesian stiffness matrix, $\boldsymbol{D} \in \mathbb{R}^{6\times6}$ is the Cartesian damping matrix, $\boldsymbol{x}_r, \dot{\boldsymbol{x}}_r \in \mathbb{R}^6$ are the Cartesian end-effector pose and velocity references, $\boldsymbol{x}, \dot{\boldsymbol{x}} \in \mathbb{R}^6$ are the current end-effector pose and velocities, $\boldsymbol{J} \in \mathbb{R}^{6\times7}$ is the robot Jacobian, which describes the relationship between end-effector velocities and joint velocities, and $\boldsymbol{\tau} \in \mathbb{R}^7$ is the commanded robot joint torques. The system is critically damped so $\boldsymbol{D} = 2\sqrt{\boldsymbol{K}}$ [27].

To ensure repeatability, a null space controller is also employed [28], which drives the robot towards a desired joint configuration. The null space torque is described by:

$$\boldsymbol{\tau}_{\text{null}} = (\boldsymbol{I} - \boldsymbol{J}^T\boldsymbol{J}^{+T})(\boldsymbol{P}_N(\boldsymbol{q}_r - \boldsymbol{q}) - \boldsymbol{D}_N(\dot{\boldsymbol{q}})) \tag{7}$$

where $\boldsymbol{I} \in \mathbb{R}^{7\times7}$ is the identity matrix, $\boldsymbol{J}^{+} \in \mathbb{R}^{7\times6}$ is the Moore-Penrose pseudo-inverse of the Jacobian $\boldsymbol{J}$, $\boldsymbol{P}_N \in \mathbb{R}^{7\times7}$ is the proportional gain of the controller, $\boldsymbol{D}_N \in \mathbb{R}^{7\times7}$ is the derivative gain (damping), $\boldsymbol{q}_r \in \mathbb{R}^7$ is the reference joint configuration, and $\boldsymbol{q} \in \mathbb{R}^7$ is the current joint configuration of the robot. Also here, we selected a critical damping $\boldsymbol{D}_N = 2\sqrt{\boldsymbol{P}_N}$. The torque commanded to the low-level controller is thus $\boldsymbol{\tau} + \boldsymbol{\tau}_{\text{null}}$.

III. Experiments and Results

We separate our experiments into two main parts:

- functionality test (Sec. III-C), with the goal of demonstrating the discomfort map creation process;
- human factors experiments (Sec. III-D), with the goal of analyzing the practicality of the proposed method on untrained participants.

Ten healthy participants (8 male and 2 female) in the age range of 20-30 participated in our study. Our experimental protocol was approved by the TU Delft Human Research Ethics Committee (HREC) and all participants provided informed consent before their participation. For HREC approval, we could not induce (physical) discomfort on the participants to generate discomfort maps in the human factors experiments. Therefore, we emulated discomfort with an auditory feedback signal provided to the participant. This signal was chosen to be a beeping sound pattern, further explained in Sec. III-B. We set *a priori* an artificial reference discomfort distribution across the range of motion of our participants and asked them to recreate this reference using the proposed method in a simulated physiotherapy session, during which their shoulder was moved by the robot arm. They were not able to see the reference map, but were instead given a reference auditory signal based on this map, emulating the corresponding discomfort and dependent on their current configuration. In this way, we intended to reproduce a situation in which all of our participants would perceive the same discomfort when performing the same motion, to assess how well a patient could synthesize an actual discomfort map in the context of a real rehabilitation (with the assumption that a discomfort distribution for this case would still exist, yet unknown for both the patient and our system). As such, we instructed our participants to react to variations in the sound pattern as they would react to variations in their own physical discomfort.

A. Experimental setup

During the experiments, participants were seated in a chair, adjustable in height, with their left elbow fitted in the elbow brace attached to the end-effector of the robot arm. The starting pose for every experiment was [AR PE SE] = [0° 0° 90°], where the bent arm is parallel to the horizontal plane (see Fig. 4.I). The robot arm used is a KUKA LBR iiwa 7 R800 collaborative robot arm. The participants received visual feedback on their estimated shoulder state, the robot's reference trajectory, and their input discomfort intensity through a monitor. The participant also received the auditory signal through Bluetooth headphones, in the second part of the experiment.

For all the experiments, AR was locked to 0°, reducing the complexity of the motions to be performed. This means that the discomfort maps coincide with the discomfort distribution considered, improving the visualization of the results.

B. Discomfort-emulating Auditory Signal Protocol

As stated before, during the human factors experiments each participant received a signal emulating the reference discomfort intensity $\bar{i}(\hat{\boldsymbol{\alpha}}(t))$, retrieved from the artificial reference discomfort distribution given their current estimated shoulder pose. We chose sound feedback over visual feedback so that the participant could focus visual attention on the scene and human-robot interaction. We chose sound feedback over tactile feedback as it can be delivered in a more repeatable and clear manner. Furthermore, tactile human-robot interaction might interfere with or confuse tactile feedback. Moreover, recent research suggested that sound and pain perception share some neurological channels [29].

To convey changes in reference intensity, we considered two types of auditory signals: continuous sound or beeping sound, where the former can vary in volume/frequency, while the latter can vary the rate of the beeping. After preliminary testing, volume/frequency modulation of a continuous sound was found to be more responsive but much less clear. This may be because humans do not perceive loudness linearly, and beeping rate modulation is easier to recognize than frequency modulation. Thus, finally, we chose the beeping sound for its clarity advantage at the expense of reaction time. The auditory signal was implemented as a repeating 1 kHz beep sound with modulation of beeping rate. The time τ_b between beeps, expressed in seconds, was inversely proportional to $\bar{i}(\hat{\boldsymbol{\alpha}}(t))$, i.e. the emulated discomfort at the current estimated shoulder state $\hat{\boldsymbol{\alpha}}$, and varies according to the law:

$$\tau_b = (1 - \bar{i}(\hat{\boldsymbol{\alpha}}(t))) + \tau_0 \tag{8}$$

where $\tau_0 = 0.3$ seconds is the duration of the beep itself, constant and independent of the reference.

C. Functionality Test

The goal of the functionality test was to demonstrate the discomfort map creation process in the space of the shoulder DoFs. During this task, the robot was fully compliant, i.e., stiffness and damping parameters for the impedance control were all set to 0, and its only role was to estimate the shoulder state during the experiment. Fig. 4 shows how a discomfort map could be created autonomously by a subject during a simple motion of the left arm.

D. Human Factors Experiments

The goal of the human factors experiments was to analyze the practicality of the proposed method on untrained participants. Fig. 5 gives a general overview of the system. The experiment simulated a robotic physiotherapy session, in which the robot arm guided the participant's shoulder

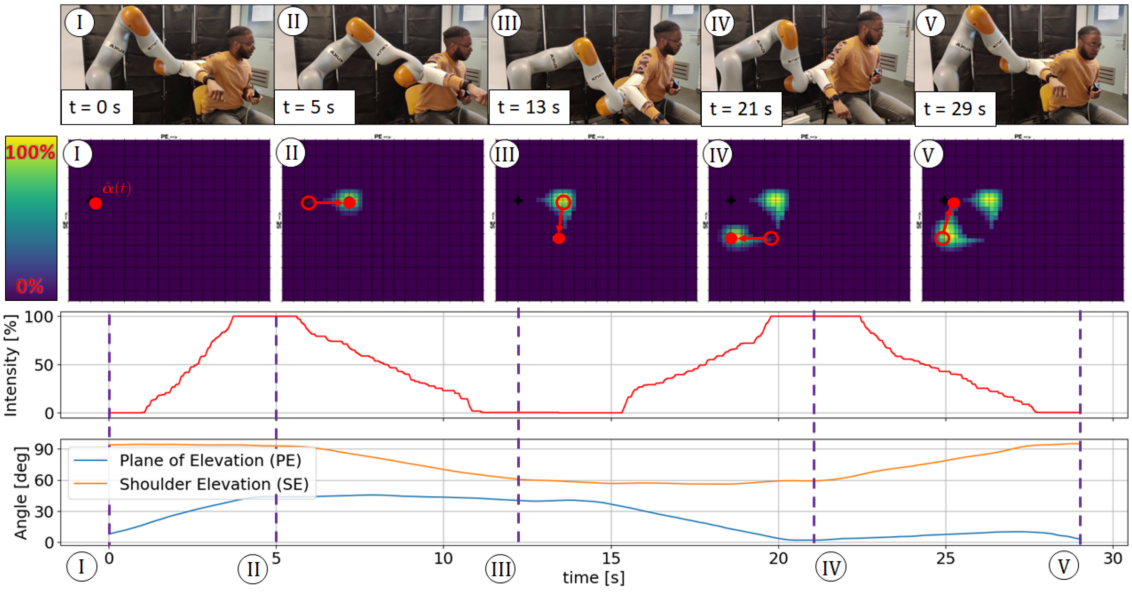

Fig. 4. Functionality test demonstrating a discomfort map creation, with snapshots taken at specific timestamps. The top row shows the robot and participant poses. The second row shows the gradual creation of the discomfort map, with the current shoulder state marked as a filled red dot and the previous as a non-filled circle. The third row shows the discomfort intensity input $i(t)$ from the participant over time, i.e., how much the push-button was pressed. The bottom row shows the PE and SE angles over time. AR is missing from this overview because, for this demonstration, the estimated AR was locked to 0. Note: The images in the first row were mirrored for demonstration purposes.

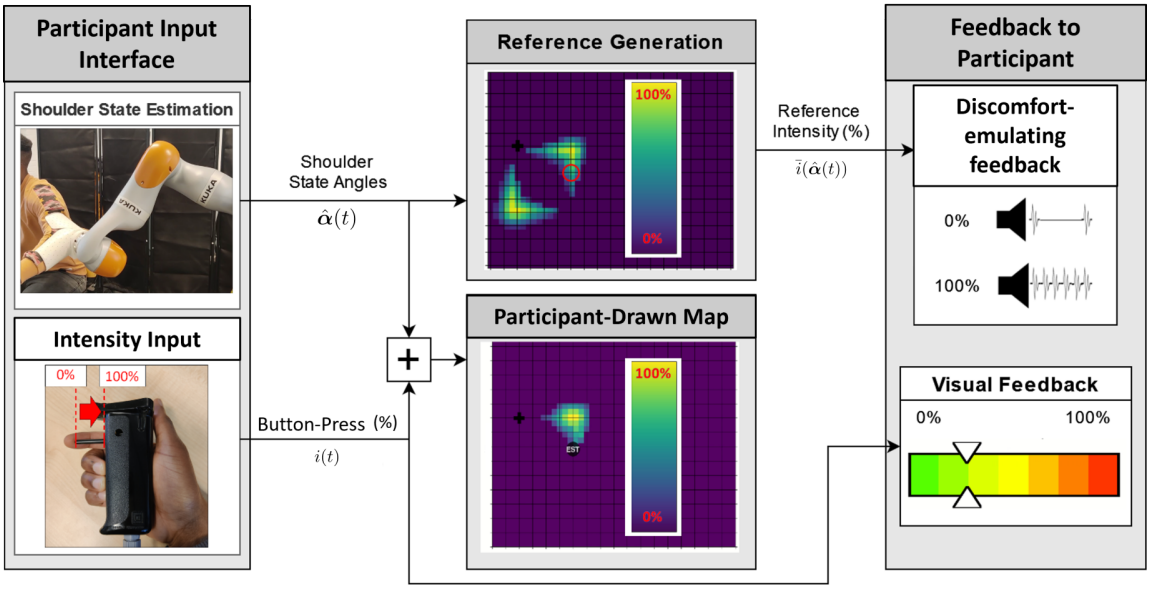

Fig. 5. Workflow for human factors experiments: Participants recreate a reference discomfort map guided by the robot and discomfort-emulating auditory feedback (Sec. III-B). The system includes participant input, reference generation, map synthesis, and feedback. Participant inputs are their shoulder state (estimated by the robot) and perceived discomfort intensity (button press). The reference discomfort intensity, derived from the reference map at the current shoulder state, modulates an audio signal, with beeping rate increasing with intensity. Feedback includes this audio signal and visual feedback of the participant's input. When drawing the discomfort map the user generates Gaussian clouds centered at their current estimated shoulder state, whose shape depends on the participant's button-press input. The drawn discomfort map is not shown to the participant, to minimize distractions during the task, and is shown here as it appears in the process of drawing it.

through a reference trajectory, while the participant was asked to passively follow the movement commanded by the robot. During the fictitious therapy, the pose of the robot's end-effector was used to estimate the current shoulder state $\hat{\alpha}$, and the beep-rate of the discomfort-emulating sound was then retrieved according to (8). Note that the combination of impedance control and physical interaction with the subject caused the robot to follow slightly different trajectories for each experiment execution, meaning that the subjects received different discomfort-emulating auditory references even when the robot's controller tracked the same trajectory more than once. The reference maps and corresponding trajectories (henceforth collectively referred to as "reference") used for the tasks are shown in Fig. 6, labeled A, B, and C.

The experiments began with a familiarization period, where the participant could freely press the button to explore how its linear displacement corresponded to the color bar for visual feedback and the beeping rate of the discomfort-emulating signal. This step was crucial for the main experiment, where participants needed to match their button press to the signal. After taking as much time as needed, they wore the arm brace and were connected to the robot. Each participant repeated every task 5 times, starting with the easiest (task A) and progressing to the most complex (task C). For safety, the robot's controller gains were tuned such that the robot could move the participant's arm while ensuring that the participant would still easily overpower it. Task repetitions were limited to prevent memorization of reference signals. Breaks were allowed, with each experiment lasting about 20 minutes.

To get quantitative insights into the similarity between the artificial reference discomfort distributions and the maps that the participants reconstructed, we employed two metrics:

- the intensity score, describing how the participant's input intensity $i(t)$ matches the reference intensity instantaneously;
- the map score, describing how the final discomfort map drawn by the participant matches the reference map.

We computed both scores as the root mean square error (RMSE) between the reference and the participants' responses. The intensity score essentially represents the average deviation between the instantaneous reference intensity $\bar{i}(\hat{\boldsymbol{\alpha}}(t))$ and $i(t)$ over the duration of the experiment. On the other hand, the map scores account for the point-wise RMSE between the map that participants reconstructed and the reference map, evaluated on regions of the maps where either was non-zero.

E. Results

Concerning the functionality test, Fig. 4 demonstrates that the combination of our hand-held device with a human-pose estimation from the collaborative robot enables the participant to transfer their perceived discomfort into a quantitative measure that is directly mapped onto the RoM of their shoulder. For what concerns the outcomes of the human factor experiment, Fig. 6 shows qualitatively the resulting discomfort maps, obtained as an average across the various participants, for each of the given trajectories. As the discomfort-emulating auditory signal was dependent on the participant's current position on the reference map, the reference they received was subject to some variability. This is visible in Fig. 7, where we present the distribution of references and participants' responses (button press) against the normalized duration of the experiments. In the same figure, it is evident that the participants reacted with some delay to the discomfort-emulating feedback. On average, this was observed to be around 1.4 seconds.

The average scores are shown in Tab. I, where lower scores indicate better performances. Performance for reference A is the best out of all references, which makes sense as it is the simplest trajectory. As expected, the presence of an error

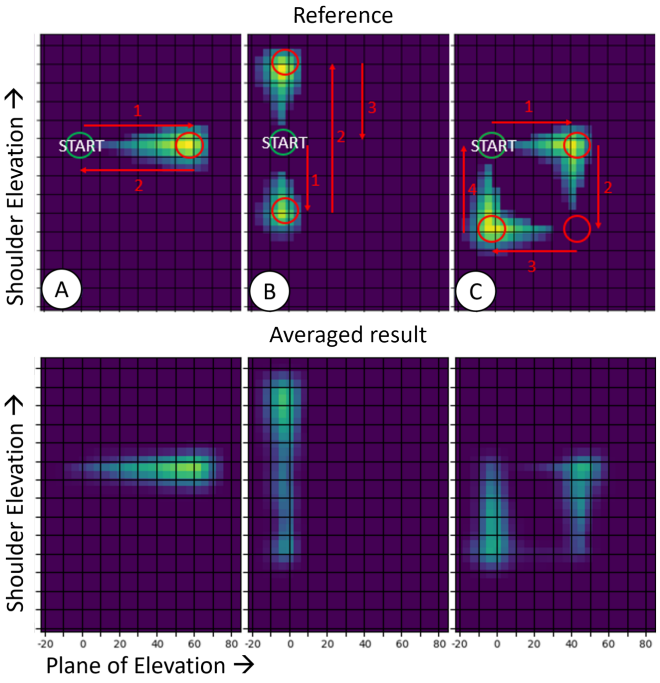

Fig. 6. The average discomfort maps created by the participants on the top row and the reference maps on the bottom row. The trajectories (A,B and C) were executed by the robot, and are here visualized in the shoulder space with red arrows, where the numbers clarify the sequence of execution for each phase of the movement.

in the tracking of the instantaneous discomfort-emulating sound directly translates into a poorer performance in the map scores. The low standard deviations reported in the table highlight that, on average, all the participants performed quite similarly across the different tasks, and the multiple repetitions for each task.

TABLE I
AVERAGE INTENSITY AND MAP SCORES, INDICATING THE RMSE BETWEEN REFERENCES AND PARTICIPANTS' INPUT

	Intensity Score			Map Score		
Task	A	B	C	A	B	C
Average	0.24	0.33	0.32	0.26	0.34	0.36
Std. dev.	0.05	0.03	0.05	0.06	0.03	0.03

IV. DISCUSSION

The human factor experiments identified important insights for the practical use of the proposed method. We can see in Fig. 6 that the averaged maps resulting from the participants' inputs do not match completely the reference (especially for tasks B and C). This is also evident when looking at the temporal relationship between the participants' input through the hand-held device and the reference discomfort-simulating feedback, in Fig. 7. It can be seen that the participants consistently underestimated the percentage of button press that was expected from them, while also introducing a significant delay. We cannot speculate if similar values would be observed when participants experience real discomfort, but we can hypothesize that these discrepancies

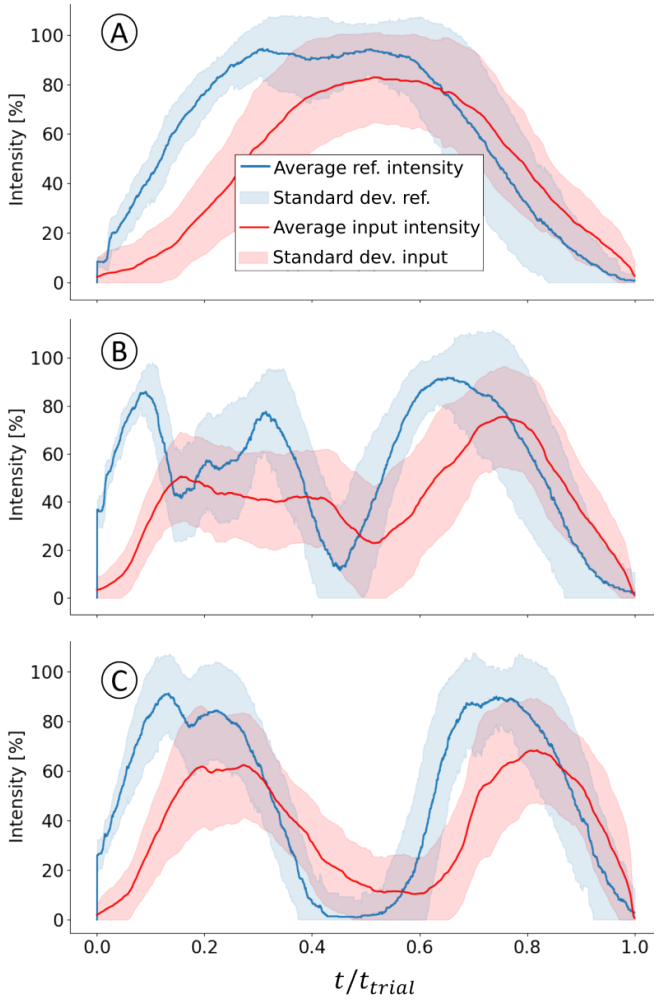

Fig. 7. Plots of the average discomfort intensity input from the participants and the average reference intensity over normalized time. It can be observed that the reference intensity is different for every trial, as the participants' shoulder movement is not precisely the same for each repetition of the task. This also entails that every trial has a different duration, and as such the data is normalized with the duration of the trial, then averaged.

could be caused by the auditory feedback as a medium to deliver the reference for the emulated discomfort. Since causing real discomfort was not possible within ethical constraints and discomfort had to be emulated, this remains a limitation of the study.

Our choice of employing a beep-rate modulation for the audio signal entails that, to detect a change, one should wait for at least 1 full beeping cycle (introducing an intrinsic delay that is dependent on the beeping rate itself). This delay, for low discomfort-emulating references, would result in $\tau_0 + \tau_b|_{\bar{i}=0} = 1.6$ seconds, which is close to the average delay of 1.4 seconds that we observed across our experiments. Thus, we believe that delays in the participants' response would be significantly reduced if they reacted to their own discomfort, rather than to a discomfort-emulating signal. However, it is important to note that, even in the case of actual discomfort, a certain amount of delay would likely be introduced anyway due to delays in the human sensorimotor system. This delay should be effectively identified and eliminated in our maps, before they can be used for real physiotherapy.

Regarding $i(t)$ consistently being lower than $\bar{i}(\hat{\boldsymbol{\alpha}}(t))$, this could be because participants tended to press the button cautiously or due to the aforementioned delay. We believe that this would not invalidate the use of our system when capturing actual discomfort, as the button press would essentially be equivalent to continuous logging of a pain-measuring scale such as the NRS, already clinically accepted for pain quantification.

There are several key benefits to the presented approach. It enables patients to quickly and accurately convey points of discomfort and their intensity to the physiotherapist, surpassing the speed of verbal communication and the precision of body language. Furthermore, the push-button interface for discomfort input presented here improves upon similar devices from the studies in [17]–[20] by being single-handed, not requiring personalization and directly integrated into a robotic system. Moreover, when integrated with a patient movement tracking system, it becomes possible to map their discomfort distribution based on the patient's pose. Though this study only addresses shoulder physiotherapy with a collaborative robot arm, this method could easily be adapted to other parts of the body or different types of robots, like exoskeletons.

In the context of robotic-assisted shoulder rehabilitation, the discomfort maps have the potential to be integrated with the strain maps [11]–[13], and make it possible to build a comprehensive representation of the mobility range of a patient while accounting for both objective biomechanical quantities and the patient's more subjective perceptions during rehabilitation. While strain maps are already personalized to the patient and the severity of their injury, discomfort maps allow further personalization that even accurate biomechanical models cannot provide to date. As an example, the discomfort maps can also consider sources of discomfort unrelated to RC tendon strain, such as inflammation in the shoulder, or different levels of pain acceptance for various patients. Furthermore, the simplicity of our pipeline enables us to easily update the discomfort maps as the therapy progresses, offering a quantitative tool that can inform the therapist, the robot-assisting device, and even the patients regarding the course of the recovery process.

Our method is also subject to limitations, mainly because we were not able to test its effectiveness in reconstructing discomfort maps that are directly related to patients' real perceived discomfort. While evaluating the quality of the discomfort maps in this real case would be challenging (as we would not have any ground truth information), future work should focus on evaluating the system as closely as possible to its real intended use. Another complication that might arise is that discomfort is likely not dependent on the shoulder state $\boldsymbol{\alpha}$ alone, but also on the speed at which the movements are performed, and on past movements as well. A system that is usable with real patients should also take into account these hystereses that are intrinsic to the physiology of the human body, and that are still an area of active research even in the medical community. Viable

options to consider may be collecting discomfort information at various speeds and reaching painful poses from different directions, to identify how discomfort perception might vary and contribute to advancing our fundamental understanding of the human body.

V. Conclusions

We developed an intuitive interface to map patient discomfort during robot-assisted shoulder physiotherapy, enabling real-time quantification of discomfort as the shoulder is manipulated by a robotic device. This system allows us to track and mitigate discomfort directly, making robotic therapies more feasible. Moreover, the discomfort maps generated provide valuable documentation of therapy progress, aiding clinicians in tailoring rehabilitation programs. Discomfort information could be integrated with our previously developed strain maps, providing a comprehensive representation of the patient's mobility range in terms of both objective and subjective measurements. Analyzing the evolution of these maps throughout the rehabilitation process offers diagnostic insights and could inform treatment selection. While our system shows promise for broader application in robotic-assisted rehabilitation of various joints, further validation in clinical settings with real discomfort is necessary to fully assess its utility.

References

[1] H. Minagawa, N. Yamamoto, H. Abe, M. Fukuda, N. Seki, K. Kikuchi, H. Kijima, and E. Itoi, "Prevalence of symptomatic and asymptomatic rotator cuff tears in the general population: From mass-screening in one village," *Journal of Orthopaedics*, vol. 10, pp. 8–12, Mar. 2013.

[2] T. Proietti, V. Crocher, A. Roby-Brami, and N. Jarrasse, "Upper-Limb Robotic Exoskeletons for Neurorehabilitation: A Review on Control Strategies," *IEEE reviews in biomedical engineering*, vol. 9, pp. 4–14, 2016.

[3] H. Østerås and T. A. Torstensen, "The Dose-Response Effect of Medical Exercise Therapy on Impairment in Patients with Unilateral Longstanding Subacromial Pain," *The Open Orthopaedics Journal*, vol. 4, pp. 1–6, Jan. 2010.

[4] "Ticking timebomb: Without immediate action, health and care workforce gaps in the European Region could spell disaster," *World Health Organization*, Sept. 2022.

[5] D. Simonetti, L. Zollo, E. Papaleo, G. Carpino, and E. Guglielmelli, "Multimodal adaptive interfaces for 3D robot-mediated upper limb neuro-rehabilitation: An overview of bio-cooperative systems," *Robotics and Autonomous Systems*, vol. 85, pp. 62–72, Nov. 2016.

[6] F. Scotto di Luzio, D. Simonetti, F. Cordella, S. Miccinilli, S. Sterzi, F. Draicchio, and L. Zollo, "Bio-Cooperative Approach for the Human-in-the-Loop Control of an End-Effector Rehabilitation Robot," *Frontiers in Neurorobotics*, vol. 12, 2018.

[7] W. Kim, J. Lee, L. Peternel, N. Tsagarakis, and A. Ajoudani, "Anticipatory Robot Assistance for the Prevention of Human Static Joint Overloading in Human-Robot Collaboration," *IEEE Robotics and Automation Letters*, vol. PP, pp. 1–1, July 2017.

[8] L. Peternel, C. Fang, N. Tsagarakis, and A. Ajoudani, "A selective muscle fatigue management approach to ergonomic human-robot co-manipulation," *Robotics and Computer-Integrated Manufacturing*, vol. 58, pp. 69–79, Aug. 2019.

[9] L. F. C. Figueredo, R. C. Aguiar, L. Chen, S. Chakrabarty, M. R. Dogar, and A. G. Cohn, "Human Comfortability: Integrating Ergonomics and Muscular-Informed Metrics for Manipulability Analysis During Human-Robot Collaboration," *IEEE Robotics and Automation Letters*, vol. 6, pp. 351–358, Apr. 2021.

[10] T. Petrič, L. Peternel, J. Morimoto, and J. Babič, "Assistive arm-exoskeleton control based on human muscular manipulability," *Frontiers in Neurorobotics*, vol. 13, 2019.

[11] J. Prendergast, S. Balvert, T. Driessen, A. Seth, and L. Peternel, "Biomechanics Aware Collaborative Robot System for Delivery of Safe Physical Therapy in Shoulder Rehabilitation," *IEEE Robotics and Automation Letters*, vol. 6, no. 4, pp. 7177–7184, 2021.

[12] S. Balvert, M. Prendergast, I. Belli, A. Seth, and L. Peternel, "Enabling Patient- and Teleoperator-led Robotic Physiotherapy via Strain Map Segmentation and Shared-authority," Nov. 2022.

[13] I. Beck, I. Belli, L. Peternel, A. Seth, and J. M. Prendergast, "Real-time tendon strain estimation of rotator-cuff muscles during robotic-assisted rehabilitation," in *2023 IEEE-RAS 22nd International Conference on Humanoid Robots (Humanoids)*, pp. 1–8, IEEE, 2023.

[14] R. B. Fillingim, "Individual differences in pain: understanding the mosaic that makes pain personal," *PAIN*, vol. 158, p. S11, Apr. 2017.

[15] R. Cowen, M. K. Stasiowska, H. Laycock, and C. Bantel, "Assessing pain objectively: the use of physiological markers," *Anaesthesia*, vol. 70, pp. 828–847, July 2015. Publisher: John Wiley & Sons, Ltd.

[16] G. D. De Sario, C. R. Haider, K. C. Maita, R. A. Torres-Guzman, O. S. Emam, F. R. Avila, J. P. Garcia, S. Borna, C. J. McLeod, C. J. Bruce, R. E. Carter, and A. J. Forte, "Using AI to Detect Pain through Facial Expressions: A Review," *Bioengineering*, vol. 10, p. 548, May 2023.

[17] E. M. Boormans, P. J. Van Kesteren, R. S. Perez, H. A. Brölmann, and W. W. Zuurmond, "Reliability of a Continuous Pain Score Meter: Real Time Pain Measurement," *Pain Practice*, vol. 9, no. 2, pp. 100–104, 2009. _eprint: https://onlinelibrary.wiley.com/doi/pdf/10.1111/j.1533-2500.2009.00260.x.

[18] A. van Wijk, F. Lobbezoo, and J. Hoogstraten, "Reliability and validity of a continuous pain registration procedure," *European Journal of Pain*, vol. 17, no. 3, pp. 394–401, 2013. _eprint: https://onlinelibrary.wiley.com/doi/pdf/10.1002/j.1532-2149.2012.00194.x.

[19] N. Schaffner, G. Folkers, S. Käppeli, M. Musholt, G. F. L. Hofbauer, and V. Candia, "A New Tool for Real-Time Pain Assessment in Experimental and Clinical Environments," *PLoS ONE*, vol. 7, p. e51014, Nov. 2012.

[20] D. M. Böing-Meßing, F. Tomschi, T. Cegla, and T. Hilberg, "The eEgg: Evaluation of a New Device to Measure Pain," *Frontiers in Physiology*, vol. 13, 2022.

[21] I. S. K. Thong, M. P. Jensen, J. Miró, and G. Tan, "The validity of pain intensity measures: what do the NRS, VAS, VRS, and FPS-R measure?," *Scandinavian Journal of Pain*, vol. 18, pp. 99–107, Jan. 2018. Publisher: De Gruyter.

[22] T. Paolucci, F. Agostini, M. Mangone, A. Bernetti, L. Pezzi, V. Liotti, E. Recubini, C. Cantarella, R. G. Bellomo, C. D'Aurizio, *et al.*, "Robotic rehabilitation for end-effector device and botulinum toxin in upper limb rehabilitation in chronic post-stroke patients: an integrated rehabilitative approach," *Neurological Sciences*, pp. 1–11, 2021.

[23] Y. Bouteraa, I. B. Abdallah, K. Alnowaiser, and A. Ibrahim, "Smart solution for pain detection in remote rehabilitation," *Alexandria Engineering Journal*, vol. 60, no. 4, pp. 3485–3500, 2021.

[24] L. Dai, J. Broekens, and K. P. Truong, "Real-time pain detection in facial expressions for health robotics," in *2019 8th International Conference on Affective Computing and Intelligent Interaction Workshops and Demos (ACIIW)*, pp. 277–283, IEEE, 2019.

[25] L. Peternel, T. Petrič, and J. Babič, "Robotic assembly solution by human-in-the-loop teaching method based on real-time stiffness modulation," *Autonomous Robots*, vol. 42, no. 1, pp. 1–17, 2018.

[26] N. Hogan, "Impedance control - an approach to manipulation. I theory. II - implementation. III - applications," *ASME Transactions Journal of Dynamic Systems and Measurement Control B*, vol. 107, pp. 1–24, 1985.

[27] A. Albu-Schaffer, C. Ott, U. Frese, and G. Hirzinger, "Cartesian impedance control of redundant robots: recent results with the DLR-light-weight-arms," in *2003 IEEE International Conference on Robotics and Automation (Cat. No.03CH37422)*, vol. 3, pp. 3704–3709 vol.3, Sept. 2003. ISSN: 1050-4729.

[28] C. C. De Wit, B. Siciliano, and G. Bastin, eds., *Theory of Robot Control*. Communications and Control Engineering, London: Springer, 1996.

[29] S. Manohar, H. J. Adler, K. Radziwon, and R. Salvi, "Interaction of auditory and pain pathways: Effects of stimulus intensity, hearing loss and opioid signaling," *Hearing research*, vol. 393, p. 108012, 2020.